

Supplemental Material: Inelastic collision dynamics of oriented NO molecules with Kr atoms

Cornelia G. Heid^a, Imogen P. Bentham^a, Razvan Gheorghe^a, Pablo G. Jambrina^b, F. Javier Aoiz^c and Mark Brouard^a

^aDepartment of Chemistry, University of Oxford, The Chemistry Research Laboratory, 12 Mansfield Road, Oxford, OX1 3TA, United Kingdom; ^bDepartamento de Química Física, Universidad de Salamanca, 37008, Salamanca, Spain; ^cDepartamento de Química Física, Facultad de Química, Universidad Complutense, 28040 Madrid, Spain

1. Integral spin-orbit branching fractions for NO + He

The QM NO + He integral spin-orbit branching fractions for the $j' = 5.5e - 10.5e$ final rotational states are presented in Figure S1, along with the branching fractions for NO + Ar and NO + Kr (these are the same QM fractions as shown in Figure 7 of the main text, plotted on a larger scale). The calculations for the NO + He system were run at the same field strength as was used in the current experiments (9.2 kV/cm), using the potential energy surfaces of Yang and Alexander [1]. The fractions for NO + He span a range from about 0.3 (for $j' = 5.5e$) to 0.8 (for $j' = 10.5e$), which is substantially larger than for NO + Ar and NO + Kr. As discussed in the main text, this is due to the dominance of the repulsive core of the NO + He PESs, which facilitates interaction with the unpaired electron such that spin-orbit changing excitations occur overall more readily than for NO colliding with Ar or Kr. The larger branching fractions are also reflected in the more similar scales of the V_{sum} and V_{diff} potentials for NO + He compared to NO + Ar/Kr (see Figure 10 in the main text).

The dependence of the branching fractions on the initial relative orientation of the NO molecule and the He atom follows the same trends for even and odd Δj transitions as the ones shown for NO + Ar and NO + Kr. The variations for the even Δj transitions are similar or slightly larger than the ones for NO + Ar, and larger than the ones for NO + Kr. This confirms that the orientational preferences are mainly determined by the repulsive core and, in the case of NO collisions with the heavier rare gases, are modulated by the attractive regions of the PES. The effect is relatively small for NO + Ar and more significant for NO + Kr.

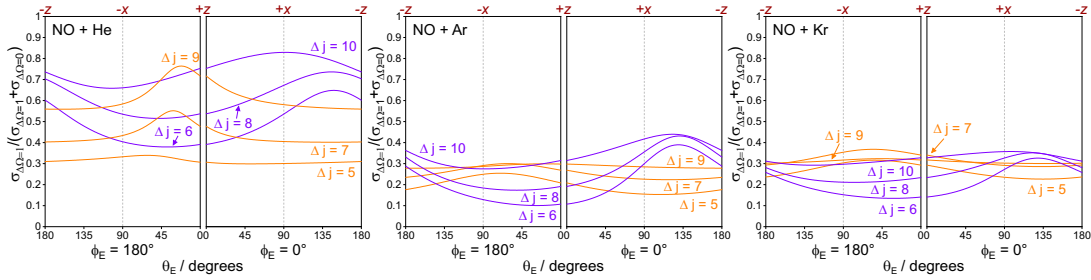


Figure S1. QM integral spin-orbit branching fractions for NO + He (left), NO + Ar (middle), and NO + Kr (right), calculated at the experimental field strength. The even $\Delta j = 6 - 10$ transitions are represented in purple; the odd $\Delta j = 5 - 9$ transitions are represented in orange. The θ_E angles corresponding to the $\pm x$ and $\pm z$ orientations are indicated at the top of the figure ($+x$ and $-z$ correspond to N-side and N-end orientation, and $-x$ and $+z$ correspond to O-side and O-end orientation, respectively).

2. Differential spin-orbit branching fractions for NO + Kr

Figure S2 shows contour plots of the differential branching fractions for NO + Kr scattering into $j' = 5.5e - 10.5e$. The x-axis in the figure is identical to the x-axis for the integral branching fractions in Figure 7 of the main text. The y-axis shows the scattering distribution as a function of scattering angle θ , which, at a given orientation, corresponds to the DCS. Red areas indicate a stronger contribution of the spin-orbit changing transitions, while light yellow areas indicate a preference for spin-orbit conserving transitions. The maxima of the fractions for odd Δj transitions (left-hand side) extend over a long range of initial orientations, and are relatively high in the more backward scattered direction ($\theta \geq 90^\circ$), where the spin-orbit conserving transitions have little intensity. This results in modest variations in the integral branching fraction as a function of initial orientation for the odd Δj states. For the $\Delta j = 6, 8$ transitions (right-hand side), the maxima are located between the $+x$ (N-side) and

$-z$ (N-end) orientations, and the minima between the $-x$ and $+z$ orientations, resulting in more pronounced maxima and minima in the integral branching fractions for these two states (see Figure 7 in the main text). The $\Delta j = 10$ transition exhibits an additional broad maximum that extends from the $-x$ orientation (at $\theta \sim 130^\circ$) and makes the minimum in the integral branching fraction shallower compared to $\Delta j = 6, 8$.

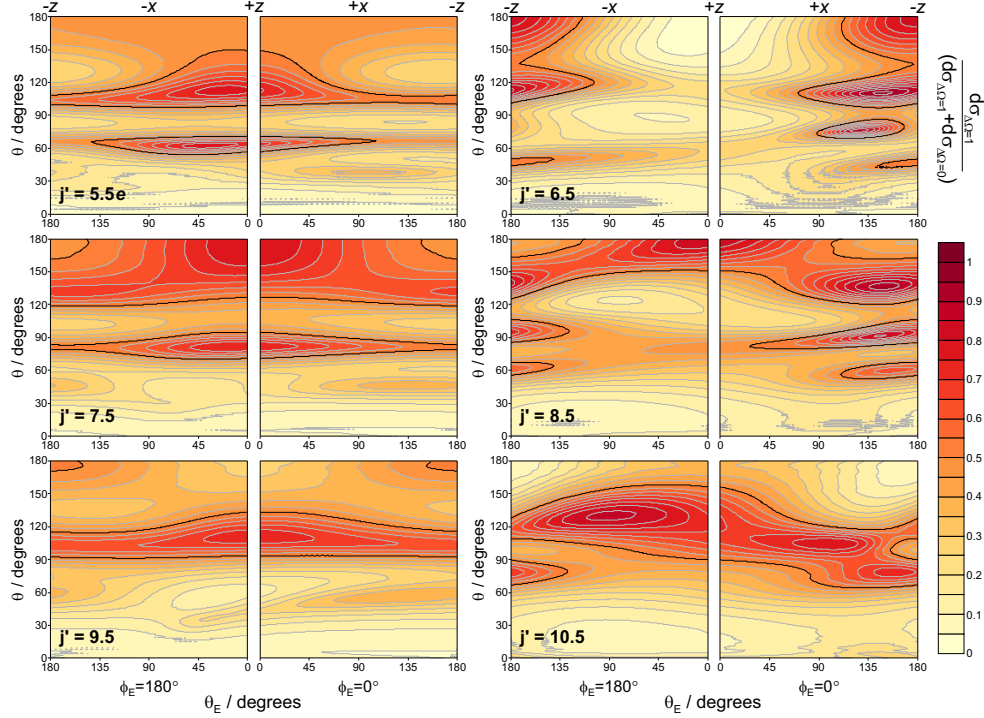


Figure S2. Contour plots of the differential spin-orbit branching fractions for NO + Kr scattering into $j' = 5.5e - 10.5e$. The fractions are shown as a function of θ (y-axis) and θ_E (x-axis), with $\phi_E = 0^\circ$ on the right-hand side and $\phi_E = 180^\circ$ on the left-hand side of each panel. The θ_E angles corresponding to the $\pm x$ and $\pm z$ orientations are indicated at the top of the figure. The black contour indicates a branching fraction of 0.5. The calculations were run at the experimental field strength and averaged over the experimental collision energy distribution with a mean of 612 cm^{-1} .

3. Comparison of the A' , A'' , and sum PES contours for NO + Ar and NO + Kr

While the attractive regions of the PES play a crucial role in the more forward scattered region for spin-orbit conserving collisions, the repulsive parts of the PES become important for backward scattering and excitations into the spin-orbit changing manifold. As observed in Figure 8 of the main text, the DCSs for the spin-orbit changing transitions look very similar for NO + Ar and NO + Kr, whereas the DCSs for the spin-orbit conserving manifold are distinct for the two systems. Figure S3 shows the PES contours for the A' , A'' , and sum potentials at the respective experimental collision energy for NO + Ar (orange line) and NO + Kr (purple line). Due to the larger mass and its higher polarisability, the repulsive core of the Kr potential extends a little further than the Ar core. However, otherwise, the specific shape of the contours for the two systems is essentially identical. This supports our interpretation that the spin-orbit changing transitions are governed by the repulsive parts of the PES. Furthermore, since for spin-orbit changing transitions the A' potential, in which the unpaired electron lies within the plane of the NO and the rare gas and is located closer to the N-end (which is why the N-end is wider than the O-end on the A' PES), is particularly important, collisions towards the N atom

are overall more efficient in promoting a change in spin-orbit quantum number.

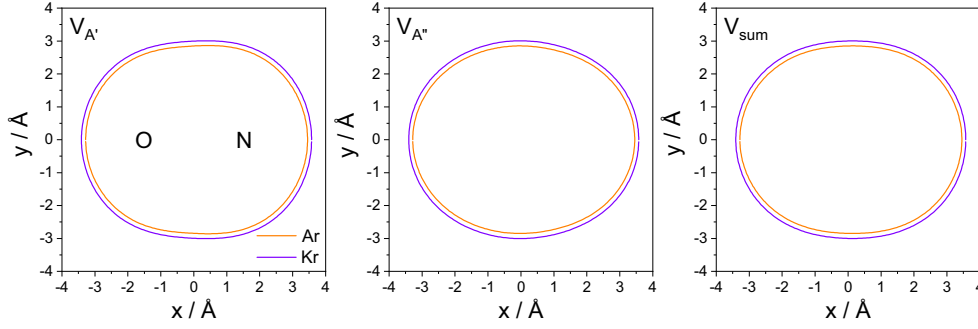


Figure S3. A' , A'' , and sum potential contours for the Ar (orange) and Kr (purple) systems at the respective experimental collision energy (651 cm^{-1} for NO + Ar, 612 cm^{-1} for NO + Kr). The N-end and O-end of the NO molecule are indicated in the left panel.

4. Unoriented, oriented, maximised, and minimised differential cross sections

The differential cross sections for oriented molecules (Equation (4)) scattering into an e final rotational state are composed of the scattering amplitudes for the pure $f \rightarrow e$ and $e \rightarrow e$ transitions (Equations (5)-(7)). In the absence of an orientation field, the DCS for a pure transition is proportional to the square of the scattering amplitude for that transition. In the presence of a field, the isotropic DCS is equivalent to orientation along the scattering frame's y -axis, for which the second and third terms in Equation (4) vanish. It is proportional to the sum of the squares of the scattering amplitudes for the pure transitions, weighted by their corresponding mixing parameters, α and β , respectively (see Equation (5)). The isotropic spin-orbit conserving DCSs for $j' = 9.5e - 12.5e$ in the presence of an infinite electric field are shown in Figure S4 as the black trace. For reference, the DCSs for the pure $f \rightarrow e$ (green) and $e \rightarrow e$ (brown) transitions are included in the first column. Since the contributions of the two Λ -doublets are equal at infinite field (*i.e.* $\alpha = \beta = 1$), the isotropic distribution is exactly the average of the pure $f \rightarrow e$ and $e \rightarrow e$ DCSs.

For an arbitrary orientation of the four-rod assembly and scattering within the plane of the molecular beams, the two opposite geometries have complementary θ_E and ϕ_E angles. For example, if orientation A is defined by $\theta_{E,A}$ and $\phi_E = 0^\circ$, the angles of its opposite orientation are $180^\circ - \theta_{E,A}$ and $\phi_E = 180^\circ$. Using these relations, Equation (4) simplifies to

$$[d\sigma(\theta)]_{\theta_E=0^\circ/180^\circ}^{\phi_E=0^\circ/180^\circ} = \frac{\sigma_{\text{iso}}}{2\pi} \left[R_0^{(0)}(\theta) \pm |\alpha\beta| \left(\cos \theta_E R_0^{(1)}(\theta) \pm \sqrt{2} \sin \theta_E R_1^{(1)}(\theta) \right) \right]. \quad (\text{S.1})$$

The second and third terms in Equation (S.1) arise from the initial orientation of the molecules in the electric field and quantify the deviation of the 'oriented' DCS from the isotropic DCS contained in the first term. The deviations for the two orientations in each case are equal in amplitude, but opposite in sign. This is illustrated in the second and third column of Figure S4 for the side-on and the end-on orientations, respectively, and in the fourth column for the maximised and minimised DCSs, which necessarily need to have opposite orientations.

For the odd $\Delta j = 9, 11$ transitions, the $+x$ and $-x$ orientations (column 2) are close to the maximised and minimised DCSs (column 4), respectively, while the $+z$ and $-z$ orientations (column 3) more closely match the maximised and minimised DCSs for the even $\Delta j = 10, 12$ transitions ($\Delta j = 12$ is somewhat less clear as the system enters the classical regime in which

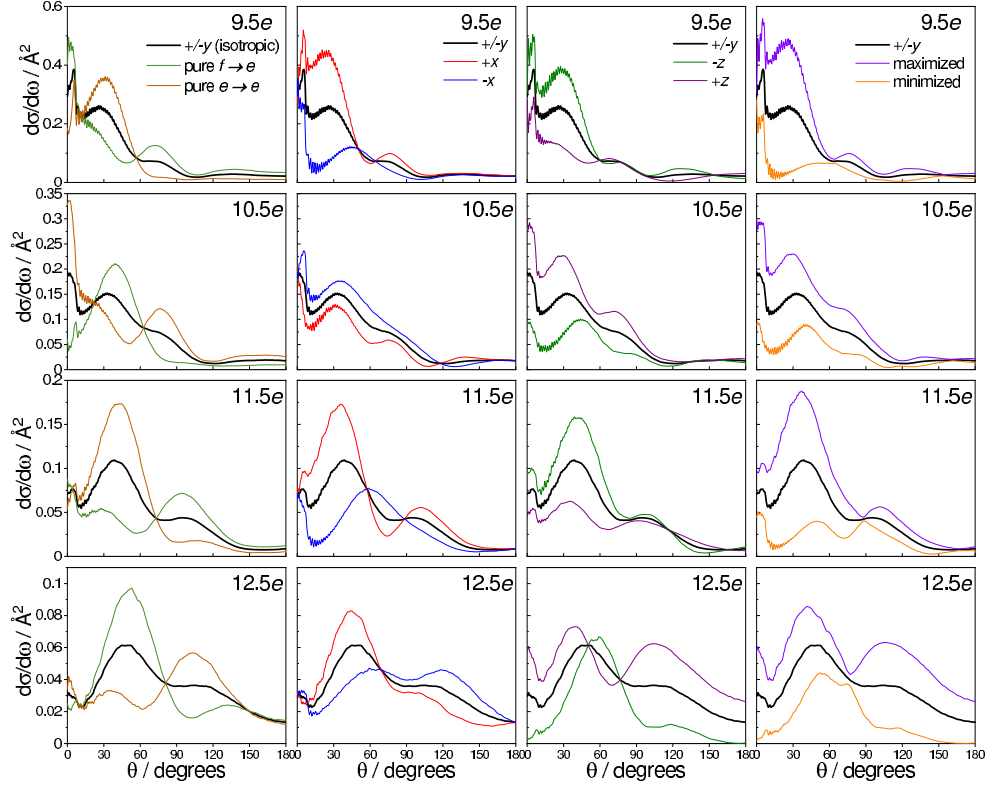


Figure S4. Comparison of the isotropic scattering distributions at infinite field (corresponding to y-axis orientation and shown in black) with the pure (field-free) $f \rightarrow e$ and $e \rightarrow e$ cross sections (column 1), as well as the x-axis (column 2), z-axis (column 3), and maximised/minimised DCSs (column 4) for $j' = 9.5e - 12.5e$ in the spin-orbit conserving manifold (top to bottom).

collisions towards the N atom dominate overall). This is consistent with the discussion in the main text and our previous work on NO + Ar [2, 3], where side-on orientations were found to be generally favoured in the more forward scattered region ($\theta \leq 90^\circ$), and end-on orientations in the more backward scattered region ($\theta \geq 90^\circ$). In Figure S4, the scattering distributions for $\Delta j = 9, 11$ are more forward scattered, while the distributions for $\Delta j = 10, 12$ extend to higher scattering angles.

References

- [1] M. Yang and M. H. Alexander, *J. Chem. Phys.*, 1995, **103**, 6973–6983.
- [2] C. G. Heid, V. Walpole, M. Brouard, F. J. Aoiz and P. G. Jambrina, *Nat. Chem.*, 2019, **11**, 662–668.
- [3] V. Walpole, C. G. Heid, P. G. Jambrina, F. J. Aoiz and M. Brouard, *J. Phys. Chem. A*, 2019, **123**, 8787–8806.